A near-field measurement based method for predicting field emissions below 30 MHz in a CISPR-25 test set-up

Zongyi Chen and Stephan Frei

TU Dortmund University, Dortmund, 44227, Germany

Correspondence to: Zongyi Chen (zongyi.chen@tu-dortmund.de)

Abstract. Automotive electric components are required to pass radiated emission tests. According to CISPR-25 standard (ALSE method), an expensive anechoic chamber is needed for conducting the field emission testing. Reproducibility due to high sensitivity to chamber and setup details is poor. Alternative methods, which perform measurements without using a chamber are preferred. This paper provides an alternative pre-compliance method for predicting the fields of CISPR-25 results for frequencies below 30 MHz, based mainly on electric near-field measurements. The motivation is that common-mode current measurements or magnetic near-field measurement based methods give good field prediction above 30 MHz, but fail below 30 MHz. The proposed method applies Huygens' Principle for field prediction. The electric field distribution for the defined Huygens' surface and the equivalent currents are estimated from a small number of field measurements close to the ground plane. It is shown that the electric field can be well predicted, compared with a full-wave simulation the deviation is within 4 dB, compared with a standard antenna measurement up to 3 MHz the deviation is less than 1 dB.

1 Introduction

Due to the high integration density of complex electronic components in automobiles, electromagnetic compatibility (EMC) performance of all individual components is important, and all components are required to pass radiated emission tests. According to CISPR-25 standard (2015), the testing is conducted in an anechoic chamber, which is quite expensive and space-consuming. Reproducibility especially 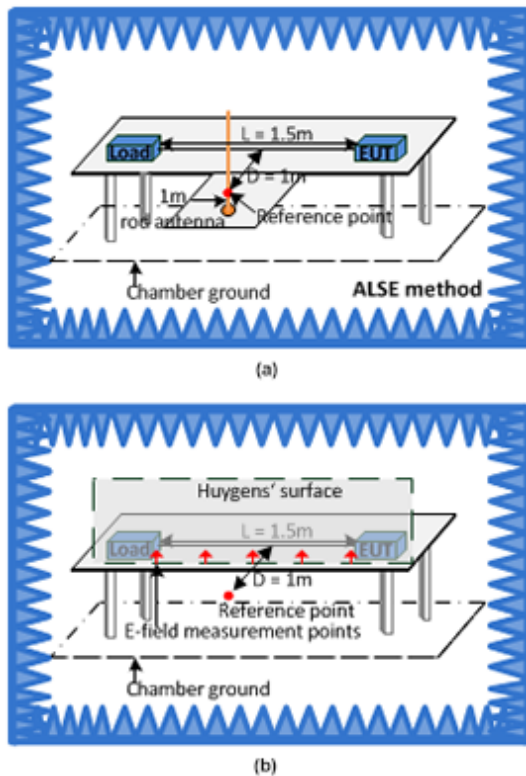at low frequencies is low (Turnbull, 2007). Alternative methods, which perform testing without an anechoic chamber, are desired.

As described in Jia et al. (2013) and Schneider et al. (2013), the measured common-mode currents along the cable bundle can be used for creating an equivalent radiation model so that the electric field at an antenna reference point can be directly calculated. Normally, creating such an equivalent radiation model needs both current amplitude and phase distributions. It has been shown by Jia (2015) that the current measurements based method fails to predict emission below 30 MHz due to the fact that the radiation model itself is too sensitive to unavoidable measurement errors. Above 30 MHz common-mode current based radiation models could reproduce quite well the CISPR-25 fields. In Radchenko et al. (2014) a Huygens' Principle based transfer function method has been investigated. The defined transfer function correlates the electric and magnetic field distributions on all mesh cells defined on Huygens' surface with the predicted antenna voltage. However, only simulated near-field distributions on Huygens' surface have been extracted, no real measured near-field distributions have been used. Also the method has been verified only in the frequency range between 30 MHz and 1 GHz. Nevertheless, it provides a new approach of using near-field distributions for emission prediction. Furthermore, near-field measurements largely minimize coupling from radiating structures far away from measurement location and impacts from measurement environment, this makes it popular for locating and reconstructing the radiation sources (Pan et al., 2015; Rodrıguez et al., 2008). In this paper near-field measurements will be performed for predicting field emission below 30 MHz in a CISPR-25 test set-up.

Below 30 MHz the standard test set-up, as depicted in Fig. 1a, the equipment under test (EUT), a load box (of-

Figure 1. (a) CISPR- 25 standard test set-up below 30 MHz, **(b)** The near-field measurements based prediction method.

ten with Artificial Network), and a connecting cable bundle ($L = 1.5$ m) are over a finite metallic table (as reference ground plane). The table is 90 cm over chamber ground. The measurement antenna (1 m rod antenna) is located at one meter distance ($D = 1$ m) in the front the cable bundle. Taking into account the particularity of field coupling in the set-up and for reduction of measurement points an unclosed Huygens' surface is proposed here, which is shown in Fig. 1b. For obtaining the field distribution along the lower edge of the Huygens' surface an electrically-small monopole antenna is used. Field measurements are executed only for observation points close to the metal table, which are represented as red arrows in the figure. This approach is chosen in order to avoid long measurement times due to many observation points and the difficulty to measure accurately local electric fields in free space. The complete field distribution and the equivalent current sources on Huygens' surface are obtained by extrapolation from the measured fields with an appropriate extrapolation function. Based on Huygens' Principle (Balanis, 1989), the electric field at antenna reference point can be directly calculated using the equivalent sources.

2 Application of Huygens' Principle

The Huygens' Principle states that the field outside of an arbitrary fictitious closed surface surrounding a radiating structure can be represented by equivalent currents on the surface. Calculation of equivalent currents from tangential electric and magnetic fields over a closed Huygens' surface are shown e.g. in Balanis (1989).

2.1 An unclosed Huygens' surface

As the measurement of a field distribution along a surrounding surface can be very time consuming and error prone, in the paper an unclosed Huygens' surface is used as shown in Fig. 1b. It is assumed that fields on surface parts that were not measured can be neglected and antenna field is dominated by the surface separating the radiation structure from the antenna. To verify the correctness of this approach a simplified CISPR-25 test set-up investigated in CONCEPT-II (2015), as shown in Fig. 2. Figure 2a gives the sketch of the model, which consists of a single cable of 1.5 m length 5 cm above an infinite perfect electric conductor (PEC) ground plane, an voltage source V_s, a source impedance Z_s and a load impedance Z_L. In Cartesian coordinate system, the cable parallels to ground plate. Figure 2b depicts the model in CONCEPT-II. In the model the finite metallic table is substituted by the infinite PEC ground plane in order to save simulation time. The replacement barely changes electric field distributions above the plate (Radchenko et al., 2014). In the simulation the parameters $V_s = 0.63$ V, $Z_s = 50\,\Omega$, and $Z_L = 10\,\Omega$, $100\,\Omega$, or $10\,\text{k}\Omega$ are chosen. The defined Huygens' surface is in parallel with XZ plane. It has length of 1.5 m and a height of 1 m. It is located in the front of cable in a distance of 0.05 m. Discretization size is 10 cm. Figure 2c shows E_{vertical} at antenna reference point (distance $D = 1$ m, height $h = 0.05$ m) from full-wave simulation and from field calculation based on equivalent currents over the defined Huygens' surface (labelled as "Huygens' method"). It can be seen the results of Huygens' method are a close match to the full-wave simulation results for the chosen Z_L. The deviation is within 0.4 dB.

2.2 Field components over defined Huygens' surface

As in simulation the fields on the closed Huygens' surface can be easily obtained, but not in the real near-field measurement. The proposed approach extrapolates from a small set of measurement points the electric and magnetic field distributions on the Huygens' surface. In order to find an appropriate extrapolation function and the required field components, the tangential electric and magnetic fields, which form the equivalent currents over the defined Huygens' surface, have been investigated.

The simplified set-up in Fig. 2 is used for investigation. When we observe E_{vertical} at antenna reference point (in
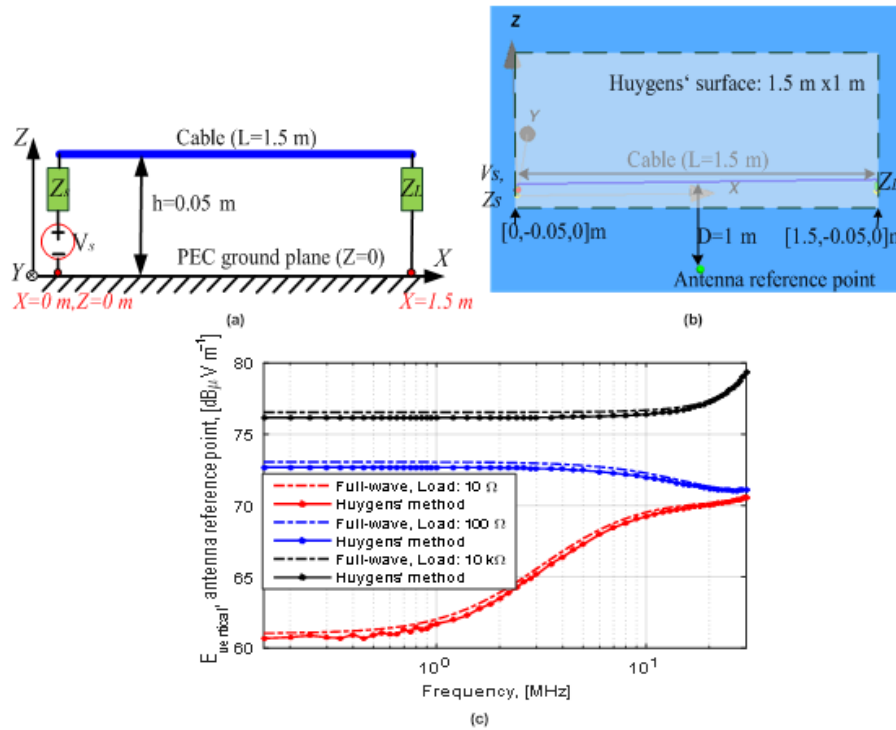
Figure 2. (a) The sketch of the simulated model, **(b)** Model in CONCEPT-II, **(c)** Comparison of full-wave simulation and Huygens' method for different load impedances.

Table 1. Deviation in dB caused by field components used for calculating electric field at antenna reference point on defined Huygens' surface by comparison with antenna field from full-wave simulation.

Load impedance	E_x, E_z, H_z, H_x	E_z	E_x	H_z	H_x	E_z and H_z	E_z and H_x	H_x and H_z
$Z_L = 10\,\Omega$	−0.31	−6.51	−354.11	−14.9	−10.09	−3.72	−2.11	−6.15
$Z_L = 100\,\Omega$	−0.37	−6.52	−356.34	−14.99	−10.23	−3.74	−2.16	−6.27
$Z_L = 10\,k\Omega$	−0.37	−6.52	−396.33	−15	−10.23	−3.74	−2.16	−6.27

Fig. 2c), almost a constant value till 10 MHz can be seen, except the case of a small load impedance (10 Ω, where the constant value is only up to 1 MHz, the inductance of the cable dominates then the voltage distribution). Taking the frequency at 1 MHz for example, Table 1 demonstrates deviations (in dB) in terms of comparison of $E_{vertical}$ at antenna reference point from the full-wave simulation and from electric field calculated using field components on defined Huygens' surface. Field components (E_x, E_z, H_x, and H_z) are used, whereas E_y and H_y are neglected, because they are normal to the defined Huygens' surface and do not contribute to radiation. As shown in Table 1, totally eight groups of field components combinations have been tested. For each group in the table, not used field components are assumed to be zero in calculation. The sign "−" means the calculated antenna field from used near-field components is smaller than full-wave simulation value. The table shows E_x has very small contribution and can be neglected. E_z is the dominant com-

ponent, which contributes more than H_x or H_z. E_z together with H_x produces a deviation within 3 dB. In further investigations shown here only E_z is considered in order to reduce the needed measurement time.

In order to observe detailed E_z distribution on the defined Huygens' surface, both magnitude and phase are shown in Figs. 3 and 4 for load impedances Z_L (= 10 Ω, 100 Ω and 10 kΩ) at 1 and 30 MHz respectively. The defined Huygens' surface is of 1.5 m in length and 1 m in height (Fig. 2), however, the shown figures are length-expanded. In Fig. 3a–c) upper figures, at 1 MHz, the dominant field distribution area is in the range $x = 0$–1.5 m, and field distribution becomes weaker along increasing heights (z from 0 to 1 m), this explains the reason a Huygens' surface of 1.5 m length and 1 m height is defined in the paper. Meanwhile, for phase distributions in the defined Huygens' surface area almost a constant value can be observed, excluding the phase jump occurs at height $z = 0.05$–0.1 m. For better observing the phase jump

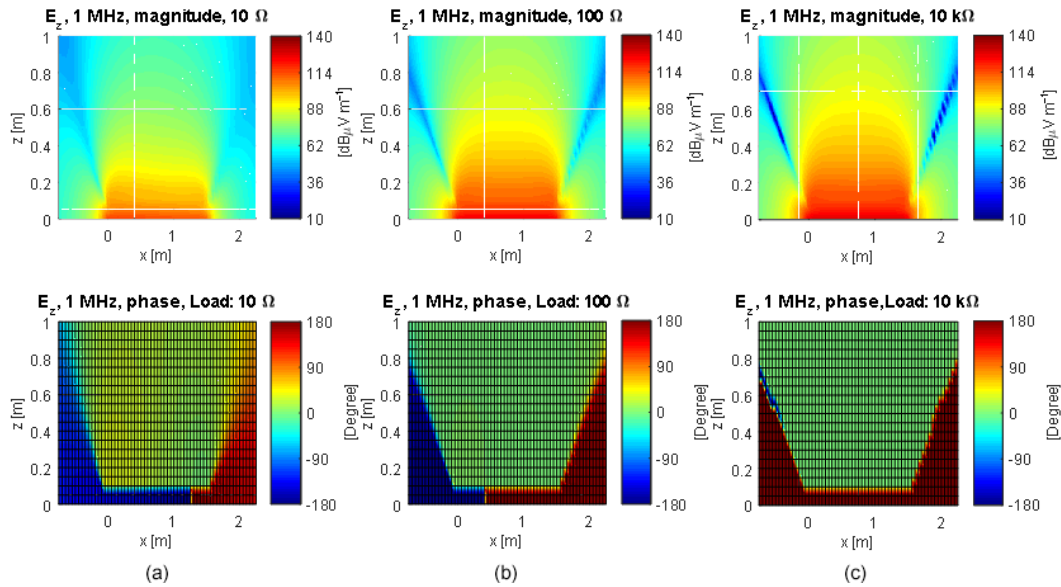**Figure 3.** E_z magnitude and phase distributions over defined Huygens' surface at 1 MHz.
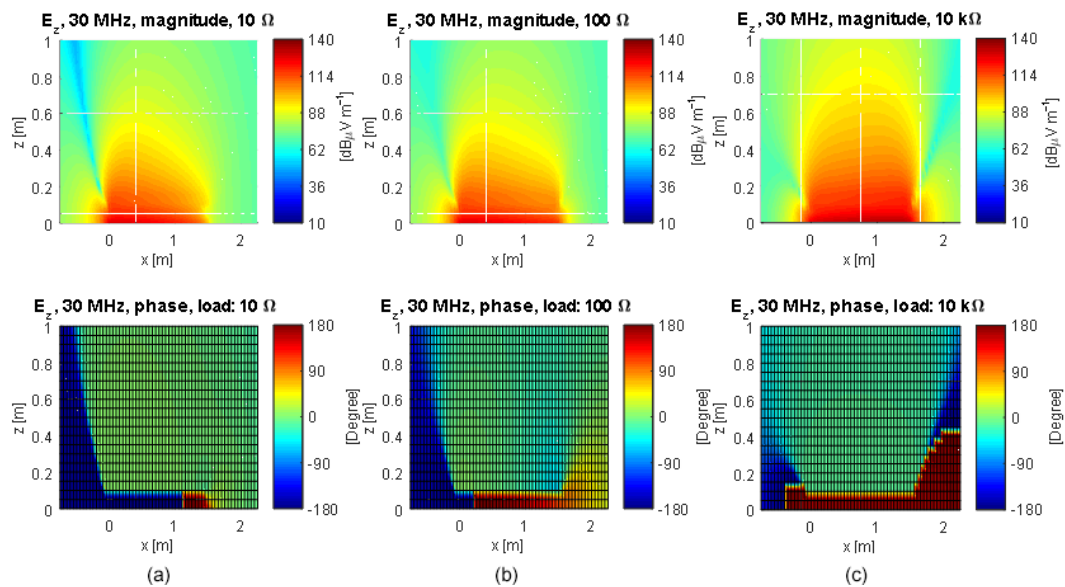

Figure 4. E_z magnitude and phase distributions over defined Huygens' surface at 30 MHz.

a dark edge colour is used. When associating this phase distribution with the result in Fig. 4 for frequency at 30 MHz, a proper assumption can be given that for the investigated model in the range $x = 0$–1.5 m, the phase jump is determined only by the set-up itself. Without employing phase distribution, for each simulated load impedance case, Fig. 5 shows the comparison of antenna field (at the antenna reference point, where 1 m distant to cable) from full-wave simulation (red line), Huygens' method (dark line, where magnitude and phase distribution of E_z over Huygens' surface are used), and Huygens' method (magenta line, where only mag-

nitude of E_z over Huygens' surface is used). It shows that the dark line matches well with the magenta line, which means calculating antenna field without using phase distribution of E_z can be acceptable. And Fig. 5 again verifies that using only E_z component on defined Huygens' surface gives the calculated antenna field, which is around 6.5 dB smaller than full-wave simulation result, as listed in the Table 1.
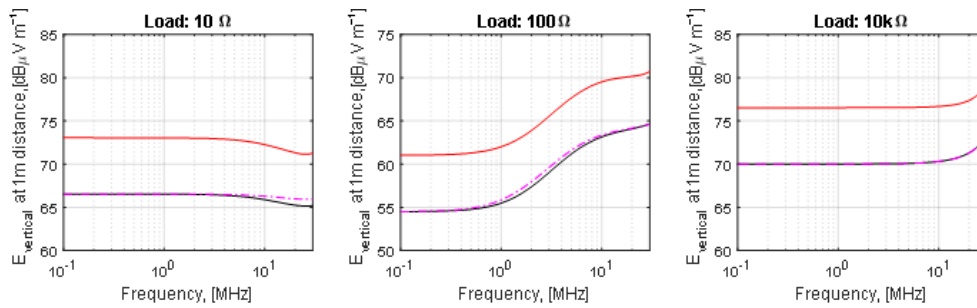
Figure 5. Comparison of antenna field from full-wave simulation, Huygens' method field calculation with/without using phase distribution of E_z over the defined Huygens' surface.
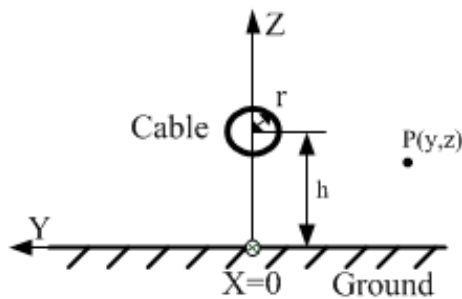

Figure 6. A sketch for electric field estimation.

Figure 7. Description of electric field estimation and interpolation on defined Huygens' surface.

3   Electric field distribution estimation

As mentioned above, conducting near-field measurements along the complete Huygens' surface is time-consuming and error prone, especially for the electric field. In the paper fields are only measured for some selected important observation points, as shown in Fig. 1b. For obtaining electric field from the connecting cable in the set-up, Fig. 6 gives a sketch of the cable in side view, which shows the cable of radius of r above ground with height h. V_p is the voltage potential on the cable. Since we are only interested in E_z over defined Huygens' surface, here only calculation for E_z is shown. By involvement of a static electric field formula, electric field at the observa-

tion P can be determined, as describes in Li (2011):

$$E_z = \frac{V_p}{\ln(2h/r)} \left[\frac{z-h}{(z-h)^2 + y^2} - \frac{z+h}{(z+h)^2 + y^2} \right] \quad (1)$$

By introducing the formula, E_z distribution tendency along the height of the defined Huygens' surface can be obtained (in the calculation, $y = -0.05$ m, $z = 0–1$ m is chosen). Later the field distribution tendency can be combined with measured electric fields for field distribution estimation on the defined Huygens' surface. The simulation model shown in Fig. 2b with $Z_L = 100\,\Omega$ is used for further analysis. Figure 7 shows the representative field points on defined Huygens' surface for description of field estimation method. Red arrows represent measured points (positions where near-field measurements with field probe are conducted, only several points are selected in order to save measurement time), blue arrows represent estimated points (the points where E_z can be estimate using Eq. (1), these points are along the height of the Huygens' surface), and green arrows represent interpolated points (to represent a proper discretization of the field distribution over the defined Huygens' surface using spline function). It should be noted that number of arrows shown in the figure doesn't stand for exact discretization size. Estimated electric field results above ideal ground at $x = 0$, 0.25, 0.75 m for frequency at 1 and 30 MHz are shown in Fig. 8. The electric field calculated from the quasi-static Eq. (1) is plotted as green curve, which matches well with electric field from full-wave simulation at $x = 0.25$ and 0.75 m for both frequency at 1 MHz (shown in Fig. 8a) and 30 MHz (shown in Fig. 8b). Deviation shown at $x = 0$ m is caused by the vertical connecting wires, which are not considered in Eq. (1). Neglecting both cable ends, it is assumed that E_z over the defined Huygens' surface follow the same distribution tendency as the electric field distribution calculated from the quasi-static formula (in Fig. 8). The electric field interpolation for the remaining field points on Huygens' surface is based on a splines function (de Boor, 1978). The process for electric field estimation and interpolation is shown in Fig. 9.
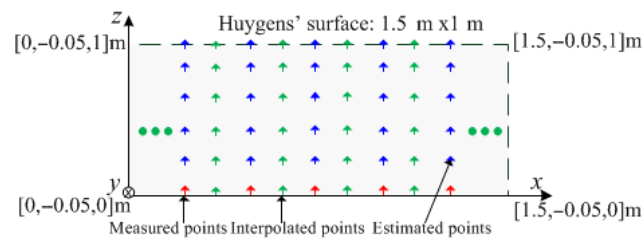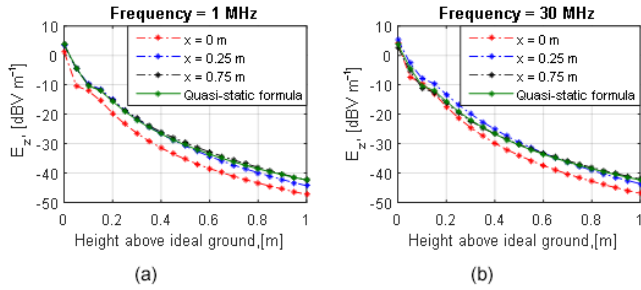
Figure 8. Comparison of simulated and estimated electric field for positions above ideal ground at $x = 0.75$ m.

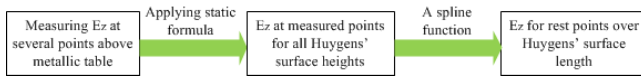**Figure 9.** Process for electric field estimation and interpolation.

Figure 10. Measurement set-up, **(a)** sketch and **(b)** picture.

4 Measurements and results

The measurement set-up is shown in Fig. 10. Figure 10a shows the sketch of the set-up, where the cable is above metallic table ($h = 5$ cm). The measurement points are symbolized with red arrows. A photo of the set-up is shown in Fig. 10b. Here a small monopole antenna is connected to an impedance converter (R&S EZ-12). Field probe is located in the front of the cable ($d = 5$ cm), as shown in Fig. 10b. In the set-up $Z_L = 10\,\Omega$ is used. The tracking generator of the test receiver (R&S ESPI 3) was applied for cable excitation, a short coaxial cable is connected to the 1.5 m cable. The applied cable is a short one, with the length less than 40 cm. Due to the short cable length we have assumed the radiation as low and neglected it. Source power has been chosen to 0 dBm.

For field probe calibration, a calibration setup was involved, as shown in Fig. 11. Figure 11a depicts the model in CONCEPT-II, a cable with length of 15 cm and radius of 1.5 mm is placed 1 cm over a metal table. Both ends of the cable are connected with a 150 Ω resistor. A field observation point M [7.5, −5, 0] cm in the model is in the center and 5 cm in the front of cable. The chosen field point is directly above infinite ground, such that only E_z component is nonzero. The field probe in Fig. 11b is located at the center of the cable and has 5 cm distance to cable center. For obtaining the probe factor, source power of 0 dBm was used as excitation for the models in simulation model and measurement just for simplification. The transfer function for field probe can be simply formulated by:

$$P_f = \frac{E_M}{V_M} \qquad (2)$$

P_f is the probe factor, E_M is simulated electric field from CONCEPT-II model, V_M is the voltage at the output of impedance converter.
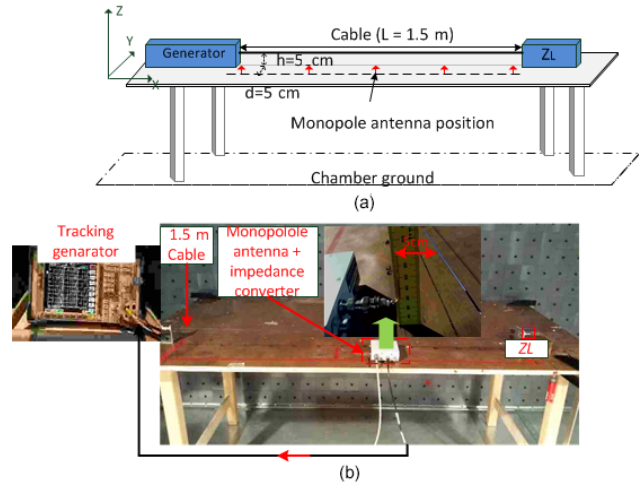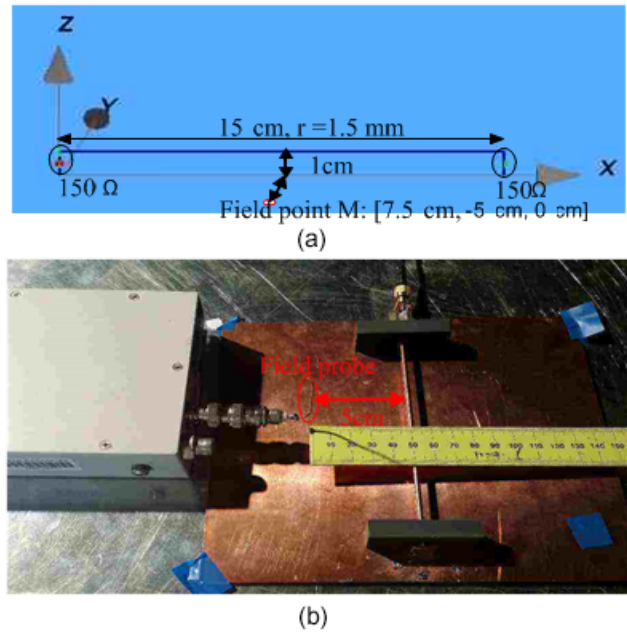

Figure 11. Field probe calibration, **(a)** calibration model in CONCEPT-II and **(b)** picture.

Figure 12 shows the comparison of E_z from field probe measurement and simulation at 1, 10, and 30 MHz. The measured electric field (red curve) is close to the simulated value (blue curve). The difference is ca. 4 dB for 1 MHz. For 10 and 30 MHz the simulated fields are a very close match to the measured fields, here the deviation is less than 1 dB. Figure 13 shows a standard antenna measurement set-up inside a shielded chamber where the 1 m rod antenna (Schwarzbeck, FMZB 1513) is located at 1 m distance away from the measured cable. The manufacturer provided antenna factor was applied for the standard antenna field calculation. Applying Huygens' Principle based field prediction method at antenna
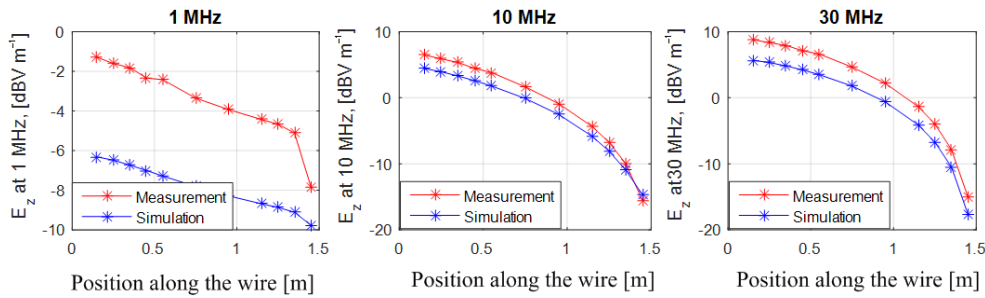
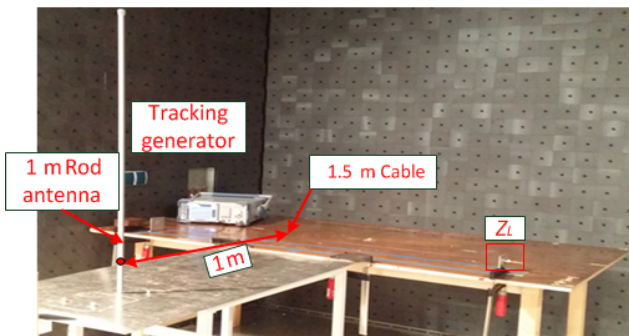**Figure 12.** Comparison of electric field measurements and simulation.

Figure 13. Standard rod antenna measurement inside chamber.

Figure 14. Comparison of Huygens' method and antenna measurement with 1 m rod antenna.

location, first, the measured E_z (in Fig. 12) has to be extrapolated to form the equivalent sources on the defined Huygens' surface. Then the antenna field can be calculated. Figure 14 shows the antenna measurement result and calculated field from Huygens' Principle based method at antenna reference point. In the figure, the red curve depicts the full-wave simulation result. The black curve shows the calculated field and the blue curve shows the standard antenna measurement.

The Huygens' method based calculated field has about 4 dB constant deviation compared to full-wave simulation. The calculate field also shows up to 3 MHz a deviation of less than 1 dB compared with the standard antenna measurement. At higher frequencies around 15 MHz the standard antenna measurement result shows a distinct resonance due to the capacitive coupling between metallic table and chamber ground. This is a well-known serious problem of the CISPR-25 method and only related to chamber properties but not to equipment under test, similar to Bongartz et al. (2009), where results shows five different chambers resulting in five different resonance frequencies.

5 Conclusions

This paper provides a near-field measurement based alternative pre-compliance method for predicting emission below 30 MHz in a CISPR-25 test set-up. The proposed method adopts the Huygens principle by defining an unclosed Huy-
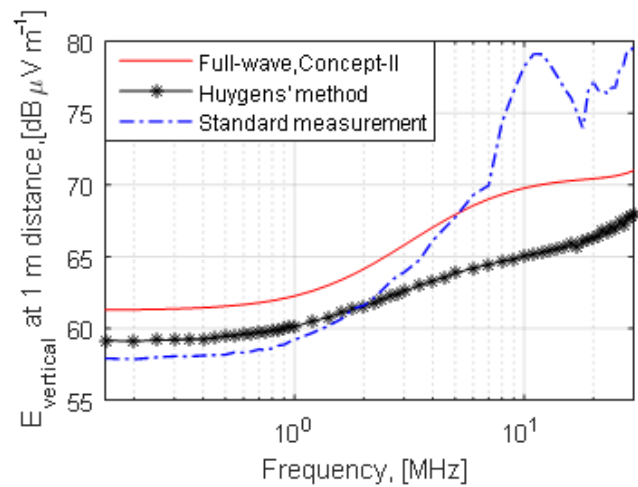
gens' surface for field prediction. Near-field measurements are only conducted for several locations over a table surface and a static electric field formula is used for field distribution estimation. The difference of the final predicted E-field at 1 m distance is within 4 dB compared with full-wave simulation. The proposed method is based on near-field measurements of a test setup and quite robust against external fields. Shielded chamber is not required for pre-compliance measurements. This way an accurate CISPR-25 1 m antenna rod result estimation can be performed in any laboratory. However, if the measurement environment is too noisy, conducting the proposed method a small chamber may be still needed.

6 Data availability

Edited by: F. Gronwald
Reviewed by: F.-W. Trautniz and one anonymous referee

References

Balanis, C. A.: Advanced Engineering Electromagnetics, New York, NY, USA, Wiley, 329–332, 1989.

Bongartz, F.-J., Deckers, J., Heina, M., Hirsch, H., Mooser, J., Nickel, J.-C., and Seiger, M.: Proposal for the validation of absorber lined shielded enclosures for CISPR 25 emission tests, Proc. IEEE Int. Symp. Electromagn. Compat., 116–120, 2009.

CISPR 25 Ed.4.0: Vehicles, boats and internal combustion engines-Radio disturbance characteristics – Limits and methods of measurements for the protection of on-board receivers, 2015.

CONCEPT-II-12.0: Technische Universität Hamburg-Harburg, available at: http://www.tet.tuhh.de/en/concept/, 2015.

de Boor, C.: A Practical Guide to Splines, Springer-Verlag, 1978.

Jia, J., Rinas, D., and Frei, S.: An alternative method for measurement of radiated emissions according to CISPR 25, IEEE Int. Symp. Electromagn. Compat., 304–309, September 2013.

Jia, J.: Current Scan Methods to Predict Radiated Emissions of Automotive Components According to CISPR 25, Ph.D. dissertation, On-board system lab, TU Dortmund, Dortmund, Germany, 2015.

Li, Z.: Electromagnetic Sensors for Measurements on Electric Power Transmission Lines, Ph.D. dissertation, Washington States University, August 2011.

Pan, J., Gao, X., and Fan, J.: Far-field prediction by only magnetic near fields on a simplified Huygens's surface, IEEE Trans. Electromagn. Compat., 57, 693–701, August 2015.

Radchenko, A., Khilkevich, V., Bondarenko, N., Pommerenke, D., Gonser, M., Hansen, J., and Keller, C.: Transfer function method for predicting the emissions in a CISPR 25 test-setup, IEEE Trans. Electromagn. Compat., 56, 894–902, August 2014.

Rodrıguez, M., Hernando, M. M., Fernandez, A., Arias, M., Alvarez, Y., and las Heras, F.: Application of the source reconstruction technique and the NF-FF transformation to estimate the EMI regulation compliance of a power electronic circuit, Applied Power Electronics Conference and Exposition (APEC), Austin (USA), 1741–1746, 2008.

Schneider, D., Böttcher, M., Tenbohlen, S., and Köhler, W.: Pre-compliance test method for radiated emissions with multiple segment transfer functions, Proc. IEEE Int. Symp. Electromagn. Compat., 605–610, August 2013.

Turnbull, L.: The groundplane resonance: problems with radiated emissions measurements below 30 MHz, EMCUK, Automotive EMC Conference, 2007.